The Cryosphere Discuss., 7, 2455–2487, 2013
www.the-cryosphere-discuss.net/7/2455/2013/
doi:10.5194/tcd-7-2455-2013

The Cryosphere Discussions
Open Access

The physical basis for gas transport through polar firn: a case study at Summit, Greenland

A. C. Adolph and M. R. Albert

Thayer School of Engineering, Dartmouth College, Hanover, NH, USA

Received: 30 April 2013 – Accepted: 2 May 2013 – Published: 7 June 2013

Correspondence to: M. R. Albert (mary.r.albert@dartmouth.edu)

Published by Copernicus Publications on behalf of the European Geosciences Union.

Abstract

Compared to other natural porous materials, relatively little is known about the physical nature of polar firn. This intricate network of ice and pore space that comprises the top 60–100 m of the polar ice sheets is the framework that forms the natural archive of past climate information. Despite the many implications for ice core interpretation, direct measurements of physical properties throughout the firn column are limited. Models of gas transport through firn are used to interpret in-situ chemical data which is retrieved to analyze past atmospheric composition. These traditional models treat the firn as a "black box," with gas transport parameters tuned to match gas concentrations with depth to known atmospheric histories. Though this method has been largely successful and provided very useful insights, there are still many questions and uncertainties to be addressed. This work seeks to understand the impact of firn structure on gas transport in firn from a first principles standpoint through direct measurements of permeability, gas diffusivity and microstructure. The relationships between gas transport properties and microstructure will be characterized and compared to existing relationships for general porous media. Direct measurements of gas diffusivity are compared to diffusivities deduced from models based on firn air chemical sampling. Our comparison illuminates the primary importance of including microstructural parameters, beyond just porosity or density, in mass transport modeling, and it provides insights about the nature of gas transport throughout the firn column. Guidance is provided for development of next-generation firn air transport models.

1 Introduction

Firn is the complex porous material, comprised of aged snow more than one year old, which separates the atmosphere from the ice cores which preserve a unique record of atmospheric history. Initiating as snow on the ice sheet surface, the pore space within the firn becomes increasingly compacted with depth due to overburden pressure, meta-

TCD
7, 2455–2487, 2013

morphism, and sintering. With this increasing compaction, the interconnected pore space ultimately becomes transformed into individual bubbles of air. Samples of the ancient atmosphere stored in these bubbles can provide insight into past climate (e.g. Severinghaus et al., 2009; Blunier and Brook, 2001). Because the air diffuses through the open pore space more rapidly than the snow turns to bubbly ice, the age of the ice and the age of the air inside the bubbles at a given depth is not the same (Schwander et al., 1993). This age difference has important implications for interpreting ice core records, particularly with respect to leads and lags between climate proxy information in the ice and CO_2 records in the bubbles, yet there remain many uncertainties in constraining this age difference because of the complexities of firn air transport (Brook, 2013).

Key to understanding the gas age–ice age difference is an understanding of the impact of the layered structure of firn itself on gas movement through the firn column. Though direct measurements of gas diffusivity, permeability and microstructure could illuminate these effects, these parameters have traditionally not been included in models of gas transport because they had not been measured. The current models rely on known histories of gas concentrations in the atmosphere combined with sampling of gas concentrations in the air from the interstitial pore space at various depths in the firn. The physical structure of the firn has not been considered. Rather, the firn is treated as a "black box", where gas diffusivity is a tuning parameter in a model to fit the measured firn air concentration with depth to known atmospheric concentration history. These tuned results are under-constrained (Trudinger et al., 2013), inconsistent with one another, and often lack a definite physical basis (Buizert et al., 2012). Witrant et al. (2012) call for measured permeability profiles in more firn air campaigns as a way to reduce the assumptions of gas transport modeling. A better understanding of the physics of firn microstructure and gas transport properties would inform these models and reduce the number of assumptions required.

Published measurements exist of firn properties that are relevant to interstitial gas transport. Albert and Shultz (2002) conducted field measurements of SF_6 diffusivity on

TCD
7, 2455–2487, 2013

the surface windpack layer at Summit using an in-situ technique developed for air–snow transfer applications. Schwander et al. (1988) and Fabre et al. (2000) made laboratory measurements of firn diffusivity, but the technique used an advective method to determine diffusivity, which introduces unnecessary assumptions; those measurements did not agree with modeled diffusivities, and they concluded that diffusivity measurements are not useful (Fabre et al., 2000). Adolph and Albert (2013) designed and verified an improved technique for direct measurements of the gas diffusivity of firn. Laboratory measurements of permeability have been made in firn, though none down through pore close off (e.g. Albert et al., 2000; Albert and Shultz, 2002; Rick and Albert, 2004; Courville et al., 2007; Horhold et al., 2009). Additionally, lattice Boltzmann modeling informed by 3-D microstructural reconstructions of firn have been used to begin to investigate gas diffusivity and permeability in firn (Freitag et al., 2002; Courville et al., 2010).

This work seeks to understand gas transport through the entire firn column on a physical basis. Transport mechanisms are investigated through direct measurement of permeability and of gas diffusivity, using a technique that was recently developed for firn (Adolph and Albert, 2013). Microstructural characteristics are determined through micro-CT scanning to provide a complete picture of the physical nature of the firn along with the metrics of gas transport. This combination of data permits assessment of the effects of microstructure on gas diffusivity and permeability. Our measured diffusivity and permeability profiles are compared with results of the firn air measurements and subsequent gas transport models. In doing so, we provide measured quantities that offer guidance for constraints which will be useful for next-generation firn air modeling.

TCD
7, 2455–2487, 2013

2 Methods

2.1 Firn samples and site location

This study focuses on firn from the top 85 m of the ice sheet at Summit, Greenland. Because of its location at the highest elevation in Greenland, ice flow generally radiates outward from Summit, such that the site is minimally disturbed by flow. Additionally, Summit has experienced a relatively constant accumulation rate in recent history (J. McConnell, personal communication, 2012). Due to its location and elevation, Summit rarely experiences melt events (Nghiem et al., 2012), and as the site of the GISP2 Ice Core project and subsequent atmospheric monitoring, there is a variety of data available. In the 2007 field season, a firn core was extracted and has remained in storage at −29 °C at the Cold Regions Research and Engineering Laboratory in Hanover, NH. The core is approximately 8 cm in diameter, and the core has has been cut into lengths ranging from 2–12 cm, based on stratigraphy. Visual inspection of firn core samples on a backlit table enabled characterization of layering in the core on a gradual scale from coarse-grained to fine-grained. Some samples are single layers which are homogeneous in their grain size, while others contain multiple layers of firn. The density of each firn samples was determined using a digital balance and dial calipers for mass and volume determination. Porosity is then calculated as $1 - \rho_{\text{firn}}/\rho_{\text{ice}}$.

2.2 Gas diffusivity measurement

Gas diffusivity is a gas transport metric that evolves from Fick's laws of diffusion. Gas diffusivity was measured on select firn samples using a technique that has been validated on glass beads and that is designed for use on firn cores (Adolph and Albert, 2013). SF_6 was used as the diffusing gas in the measurements because it is inert, and thus the results will only be affected by the geometrical properties of the firn, and not by any chemical interactions or sorption. For the measurements, the firn sample is placed in a sealed holder which is attached to a closed chamber on each side. SF_6 is injected

TCD
7, 2455–2487, 2013

into the initial chamber and then allowed to diffuse through the sample and into the exit chamber over time. Concentration is monitored in the initial chamber, and the profile of concentration over time is used to determine the diffusivity using a numerical solution for Fick's second law of diffusion:

$$\frac{\partial c}{\partial t} = D_f \frac{\partial^2 c}{\partial z^2} \quad (1)$$

where c is the gas concentration, t represents time, D_f is the diffusivity of the firn sample, and z is the position in the firn. The SF_6 concentrations are measured using a Lagus Applied Technology Autotrac 101 gas chromatograph. Diffusivity measurements were made on 46 firn core samples from depths in the ice sheet that ranged between 1.7 m to 70.7 m. Samples were determined to be homogeneous by inspection on a backlit table, and grain size in the layers were characterized on a scale from fine to coarse grained.

2.3 Permeability measurement

Permeability is defined in Darcy's law as the factor relating air flow velocity and a pressure differential across a porous medium as follows:

$$v = \frac{k}{\mu} \frac{\mathrm{d}P}{\mathrm{d}z} \quad (2)$$

Where k is permeability, v is the air flow velocity, μ is the dynamic viscosity, and P is the pressure. Permeability was measured on each firn sample from the entire firn core, from the surface down to 90 m depth. It is measured along the vertical axis of the core samples, which ranged in height from 2–12 cm. To determine permeability, the firn sample is subjected to a variety of different flow velocities, and at each distinct flow velocity, the pressure differential across the sample is measured. The permeability is calculated from Darcy's law using the measured air flow rate, pressure drop, temperature, and barometric pressure (Albert et al., 2000).

TCD
7, 2455–2487, 2013

2.4 Microstructural properties

Select firn samples were imaged using a Skyscan 1172 micro-CT scanner in a temperature controlled room held at −12 °C. The procedure used to scan the samples is described in detail by Lomonaco et al. (2011), with the only difference being the thresholding procedure. For this work, a constant threshold separating the ice phase from the pore phase was used to divide the 256 bits of greyscale: 0–89 for the ice phase and 90–256 for the pore phase. The micro-CT provides a 3-D image of the firn and the pores and also calculates a number of physical parameters which describe the microstructure of the firn. The parameters of interest are the structural model index (SMI), the specific surface area (SSA) and the average circular equivalent diameter (d_{eq}). SMI gives an indication of the concavity or convexity of the ice or pores. Positive values indicate a convex shape, and negative values indicate a concave shape. The SSA is a ratio of the surface area of the pores to the total volume of the firn sample; this can indicate the tortuosity of the firn (Lomonaco et al., 2011). d_{eq} is calculated on 2-D slices as the diameter of a circle that has the equivalent area to a given pore. The average for each of the samples imaged is taken for all of the pores in that sample.

3 Results and discussion

3.1 Gas diffusivity and permeability profiles

Figure 1 shows the profile of permeability and normalized gas diffusivity with depth. For reference, the density profile of the firn is shown in Fig. 2. The measured permeability on samples between the surface and 85 m depth ranged from impermeable at the lock in depth to $177 \times 10^{-10} m^2$ in near surface firn. The general shape of the permeability profile is the same as measured in the top ten meters on a different shallow core in earlier studies (Albert and Shultz, 2002). The peak in permeability occurs below the firn surface, due to post-depositional metamorphism on aged firn and lower

TCD
7, 2455–2487, 2013

permeability of the thick windpack surface layer (Albert and Shultz, 2002). Gas diffusivity was normalized by dividing the measured gas diffusivity of the firn sample (D_f) by the free air diffusivity of SF_6 at experimental temperature and pressure conditions (T = 260 K, P = 1000 mbar, D_a = 0.0836 $cm^2 s^{-1}$) (Matsunga et al., 2002). The normalized results ranged from 0.02 in the lock in zone to 0.58 in near surface firn. Albert and Shultz (2002) determined the normalized diffusivities of near surface windpacked snow to be 0.57 and 0.64, which are comprable to our near surface firn measurements. Overall, the diffusivity profile does not exhibit the same shape as the permeability profile, indicating that these two parameters do not have a constant linear relationship, and that these two gas transport metrics are dependent on different microstructural properties.

3.1.1 Comparison of measured permeability and gas diffusivity to simulated results

Numerical investigations of gas diffusivity and permeability based on lattice Boltzmann modeling have been published; Freitag et al. (2002) used three dimensional reconstructions of firn as inputs for modeling to calculate gas diffusivity and permeability. The reconstructions were developed from samples that were approximately 3×4×4 cm, and were created by using a microtome to remove one layer at a time and imaging between each cut to reconstruct a 3-D model. Their results showed that permeability was related to porosity (ϕ) by a power law with exponent 3.4, and diffusivity was related to porosity by a power law with exponent 2.1 as follows:

$$k = 10^{-7.7}\,m^2\,\phi^{3.4} \quad (3)$$

$$\frac{D_f}{D_a} = \phi^{2.1} \quad (4)$$

Our measurements are compared to these relationships in Fig. 3. The relationships obtained from modeling underestimate the measured permeability and gas diffusivity,

TCD
7, 2455–2487, 2013

particularly at high porosities for permeability and over most of the porosity range for diffusivity. The Freitag et al. (2002) samples were from a different site in Greenland, and so the model results are likely to be site-specific. It is also possible that the smaller sample size of the firn from the imaging used to drive the modeling may not constitute a representative elementary volume or may not represent spatial variability found in firn (e.g. Fabre et al., 2000); however, the chronic underestimate of the gas diffusivity values by the model seems to indicate an inability of the model to accurately capture the phenomena in the general case for firn. The primary element of the relationships in Eqs. (3) and (4) is porosity. It is evident that porosity alone cannot be used to predict the permeability or gas diffusivity, which is why full microsctructural data was used for the lattice Boltzmann modeling. Porosity alone cannot describe the microstructure, and aspects of the microstructure are likely to have a direct impact on transport properties.

3.1.2 Influence of microstructure on permeability and gas diffusivity

By comparing the diffusivity and permeability to measured microstructural parameters determined by 3-D micro-CT imaging, the relative effects of the different tomographic parameters can be seen. To determine these effects on the overall gas transport metrics, a linear standard least squares fit model was developed for the permeability and for the gas diffusivity profiles based on the inputs of porosity, specific surface area and average circle equivalent pore diameter (d_{eq}), as depicted in Fig. 4. The model for gas diffusivity was developed for normalized diffusivity in order to facilitate use of the results for other gases. The model for permeability employed the base-10 logarithm of permeability in order to obtain linear dataset. The models yielded linear fits with $R^2 = 0.89$ ($p < 0.0001$) for permeability and $R^2 = 0.91$ ($p < 0.0001$) for diffusivity (see Fig. 4), and the resulting relationships for Summit are as follows:

$$\frac{D_f}{D_a} = -0.003 + 0.694(\phi) - 0.006(\mathrm{SSA}) + 0.037(d_{eq}) \quad (5)$$

$$\log(k) = 0.441 + 5.151(\phi) - 0.104(\mathrm{SSA}) - 0.426(d_{eq}) \quad (6)$$

TCD
7, 2455–2487, 2013

Effect tests were implemented to determine the relative importance of each of the different physical property inputs. The results are shown in Table 1. Porosity is the main factor affecting both gas diffusivity and permeability, with an effect of 86.7 % and 59.7 %, respectively. For the relationship for gas diffusivity, the effects of SSA and pore size are not statistically significant to the diffusivity prediction. However, SSA and pore size play a larger role in the permeability outcome than they do for diffusivity. In particular, SSA accounts for 31.3 % of the variability in permeability. Porosity is a coarse measurement of the amount of air space in the firn, whereas SSA and average pore diameter are a reflection of the arrangement of the pore space. Permeability is more sensitive to the arrangement of the firn and the pores than is the gas diffusivity. This difference in sensitivity was also found to be true in other porous materials (Garboczi, 1990), including cement pastes, where permeability was significantly more dependent on pore size than was diffusivity (Garboczi and Bentz, 2001).

3.1.3 Comparison of permeability and gas diffusivity relationships to general results for porous media

In the study of generalized porous media, previous relationships including other microstructural properties beyond porosity have been developed to relate diffusivity and permeability. Two particularly well known relationships are the Kozeny–Carman and the Katz–Thompson theories. The Kozeny–Carman approximation is derived by assuming a collection of cylindrical tubes, and solving for the flow through them. The solution is generalized by multiplying by a coefficient to be determined experimentally. It has proven particularly useful in the study of powders (Garboczi, 1990; Schwartz et al., 1993). The formula is as follows:

$$k = \frac{\left(\frac{V_p}{S}\right)^2}{2F} \approx \frac{1}{2}\phi\left(\frac{1}{\mathrm{SSA}}\right)^2\left(\frac{D_f}{D_a}\right) \tag{7}$$

TCD
7, 2455–2487, 2013

where V_p/S is the inverse of the specific surface area and F is the formation factor, which is equal to in inverse of the normalized diffusivity, D_f/D_a (Schwartz et al., 1993). The Katz–Thompson approximation is developed from percolation theory and requires a critical pore diameter and a measure of the sample conductivity of the pore space, which is then linked to the formation factor (Garboczi, 1990). The Katz–Thompson approximation is as follows:

$$k = \frac{cd_c}{F} \approx cd_{eq}\frac{D_f}{D_a} \tag{8}$$

where d_c is the critical pore diameter and c is a calculated (not experimentally determined) constant. The critical pore diameter is the minimum diameter present of the pores that are connected through the whole sample. Critical pore diameter is typically determined by mercury intrusion experiments (Garboczi, 1990); in this study, due to the lack of a parameter equivalnt to the critical pore diameter, we approximate it using an average equivalent circle pore diameter determined through micro-CT scanning. Using this approximation, the Katz–Thompson theory provides an upper bound on permeability, and is not expected to give an exact approximation. Figure 5 shows the measured permeability as compared to these two different approximations. Though the general shape of the measured permeability curve is matched by the approximations, there are large deviations (up to an order or magnitude) between the two. The percent error bewteen measured and approximated permeability is shown in Fig. 6; the large and non-uniform relative errors indicate that the Kozeny–Carman and Katz–Thompson formulas should not be implemented directly.

3.1.4 Variations in the relationship between diffusivity and permeabilty with depth

The inability of general relationships for porous media to predict the relationship between diffusivity and permeability for polar firn leads to our hypothesis that considering

TCD
7, 2455–2487, 2013

changes in overarching strucutre over various depth intervals may reveal relationships that differ throughout the firn column. An investigation of the microstructure using micro-CT measurements on some of the fine-grained layers at various depths from this core were reported in Lomonaco et al. (2011). Using this information can inform our understanding of the relationship between diffusivity and permeability, which is evidently nonlinear (see Fig. 7). One control on this relationship is the relative shape of the ice and pore matrix as indicated by the structural model index (SMI). A positive SMI correlates to a convex structure (mainly pore space surrounding particles of ice), and a negative SMI correlates to a concave structure (mainly ice surrounding pockets or channels of air) (Lomonaco et al., 2011).

At Summit, in the near-surface firn down to 20 m within the ice sheet, the ice forms mainly convex structures, whereas in the deeper parts of the firn column, below 40 m, the ice has mainly concave structures (Lomonaco et al., 2011). In terms of gas transport, this indicates a switch from gas traveling around particles to traveling through tortuous channels. In the region where the firn structure is more concave (below 40 m), diffusivity and permeability are linearly related with an R^2 value of 0.875. In the region above 20 m, SMI is positive, and the best fit between diffusivity and permeability can be achieved using a polynomial, though we do not suggest that a polynomal fit fully represents this relationship. The ratio of permeability to diffusivity in near surface firn, though not well-constrained, is much higher than the same ratio near pore close off. This is due to the logarithmic trends of the average pore size and SSA with depth (see Fig. 8). Because permeability is more sensitive to these microstructural properties, the rapid change in d_{eq} and SSA near the firn surface has a larger effect on permeability than on diffusivity, which we have shown to be much more dependent on porosity than the other two parameters. This results in a larger spread in permeability than in diffusivity. In the region between 20 and 40 m, SMI hovers around zero; porosity is decreasing with depth and the structure of the pores is becoming more convex, but the pore size and SSA are no longer changing as drastically. Though this causes decrease in the diffusivity across the depth, the permeability is relatively constant. The

TCD
7, 2455–2487, 2013

three distinct phases of the relationship between diffusivity and permeability clearly indicate a variable sensitivity to pore geometry that will likely differ between sites. Once the microstructure is known, understanding these sensitivities will help to translate gas transport findings to different sites with fewer assumptions.

3.2 Comparison to firn air modelling

Direct measurements of diffusivity and permeability and their relationship to microstructure deepen our understanding of firn as a porous material, but it is in the application of these measurements to firn air modeling where these metrics can inform our methods for reconstructing gas age–ice age differences. We now investigate the comparison of our laboratory-determined diffusivities to the tuned molecular diffusivity profiles from firn gas transport models. Our direct diffusivity measurements are compared to two modeled CO_2 diffusivity profiles from Summit, Greenland developed by Buizert (personal communication, 2013) and Battle (personal communication, 2012). To facilitate this comparison, our laboratory measurements of diffusivity are normalized by dividing by the free air diffusivity of SF_6 at experimental temperature and pressure conditions, and the CO_2 diffusivity profiles are normalized by the free air diffusivity of CO_2 at Summit temperature and pressure conditions. With $T = -31.4\,^{\circ}\mathrm{C}$ and $P = 665\,\mathrm{hPa}$ (Schwander et al., 1993; Witrant et al., 2012), the free air gas diffusivity of CO_2 at Summit is $D_{CO_2,air} = 0.18\,\mathrm{cm}^2\,\mathrm{s}^{-1}$ (Matsunga et al., 1998). In Fig. 9 we show the comparison of measured and modeled diffusivity as the ratio of diffusivity in firn (D_f) to the diffusivity in free air (D_a). Our results are similar to what was shown in Fabre et al. (2000); modeled parameterizations of diffusivity result in much higher values than what is measured on discrete firn samples in the laboratory. Figure 9 shows three demarcations between regions in the firn where we will address the causes of difference between measured and modeled results.

The first region includes the near surface firn above 5 m. The measured and modeled results vary significantly (see Fig. 9, region 1), but the comparison is complicated by the known presence of alternate gas transport processes. In the near surface firn, con-

TCD
7, 2455–2487, 2013

vection and diffusion are the two dominant modes of gas transport, depending on the wind-forcing of air flow through near-surface snow (e.g. Sowers et al., 1992). Though there are a variety of definitions of the convective zone, we will define it as the region in the firn where gas transport is at least sometimes dominamted by convection, as determined by the relative convective and diffusive velocities. Albert and Shultz (2002) conducted in-situ tracer gas measurements at Summit to demonstrate that ventilation can occur, even under light wind conditions, in high-permeability layers buried 15 cm below the surface, and that the firn in summer at Summit is sufficiently permeable to permit wind-induced air flow as deep as 5 m in the firn under very strong winds. Convective zone thickness can also be determined using δ^{15}N measurements from firn air campaigns (Kawamura et al., 2006). When the air is mixed due to convection, the nitrogen isotopes are not gravitationally fractionated. Once diffusion becomes the dominant mode of transport, fractionation occurs. Looking at profiles of δ^{15}N with depth shows the point at which the heavier nitrogen isotopes start to become enriched. Using this technique, a convective zone of approximately 5 m was found at Summit in the 2007 field season (J. Severinghaus, personal communication, 2012). D_{eddy} was parameterized by the following equation to match the δ^{15}N results:

$$D_{\mathrm{eddy}} = 3.0 \times 10^{-5} e^{-z/2.1} \quad (9)$$

This parameterization is shown in Fig. 10 along with the measured diffusivity profile of SF_6 converted to appropriate Summit temperature and pressure conditions. Though the variability of diffusivity is high in the near-surface firn due to the nature of the firn layering, it appears that molecular diffusion (at least for SF_6) does indeed dominate over the convection as represented by "eddy diffusion" at a depth of approximately 5 m.

The convection that occurs in the near surface firn and the high variability caused by layering are at the root of the differences between the measured and modeled profiles of molecular diffusion. Modeled diffusivity is also not well-constrained in the near surface. This lack of constraint is investigated in detail by Trudinger et al. (2013), and it is partially due to the fact that there may be multiple modeled diffusivity profiles that

TCD
7, 2455–2487, 2013

could provide the same concentration vs. depth output. This complication is known as "equifinality" (Trudinger et al., 2013). These models in particular often exhibit smooth curves, when in reality, more abrupt shifts in gas transport may be occurring.

Below 5 m, there is no evidence for convection in the firn at Summit, but there is still a distinct difference between the measured and modeled diffusivities (see Fig. 9, region 2) in the firn between 5 and 60 m depth. It is also of note to point out that the two models in question disagree with each other significantly at these depths, particularly between 15 and 50 m depth. Our measurements indicate the portion of gas trasnport that is due to molecular diffusion; the models may be capturing the results of other types of gas transport, which are being included as part of the diffusive term. Though there have been suggestions for other types of gas transport in mid-depth firn such as dispersion from bubble closure and barometric pressure variations, it has been shown that these processes are neglible compared to molecular diffusivity (Schwander, 1989).

We believe that the variations between measured and modeled diffusivities in region 2 (Fig. 9) are likely caused by layering effects, lateral imhomogeneity and the time varient nature of the gas concentration profiles which are sampled to determine the modeled diffusivity. The laboratory-determined diffusivities are measured on discrete samples. While they reflect the layer from which they were obtained, they do not account for the effects of every layer in the firn column. In in-situ firn air measurements conducted in the field, a much larger volume of air is being sampled, so the net effects of layering are implicitly incorporated. The smaller size of laboratory samples also may not account for the lateral inhomogeneity in the firn. We do not expect a high degree of lateral inhomogenaity at Summit due to the fairly constant and relatively high accumulation rate, generally calm wind conditions, and radar surveys showing generally flat layering at Summit (S. Arcone, personal communication, 2013). However, some variation is inevitable in any natural material. For example at the NEEM drilling site, two boreholes drilled only 64 m apart showed variation in their structure and gas concentration profiles (Buizert et al., 2012). The differences observed at NEEM are likely due both to the fact that the firn cores there contained low-permeability ice layers (K. Kee-

TCD
7, 2455–2487, 2013

gan, personal communication, 2013) at different locations in the cores, and also that the concentration profiles are not in steady state. For example, at any site, a spatially inhomogeneous layer of low permeability may significantly slow down gas transport in one coring location, potentially leading to a higher concentration of a given chemical species. However, if that same low permeability layer is not present in a nearby coring location, the high concentration caused by retarded gas motion will not be present. In a steady state situation, these changes would not be significant. Time varience of gas concentration in the atmosphere (and subsequently in the firn) does occur. The combined effects of lateral inhomogeneity and non steady-state conditions in the field contribute to the differences between the modeled and measured diffusivities depicted in region 2 of Fig. 9.

Region 3 in Fig. 9 shows that the measured and modeled results agree fairly well at depth, though there are relatively few measurements in that range. As diffusivity approaches zero due to increased tortuosity and the closing of pore channels, all solutions must approach zero, so there is little leeway for variability in the models. Only two measurements of diffusivity were made in the region defined by firn air measurements as the lock in zone; however, our results indicate non-zero values of molecular diffusivity at those depths. Many models have found it necessary to include a diffusive term in their lock in zone in order to obtain matching concentration profiles, particularly for $^{14}CO_2$ (Buizert et al., 2012). Because there is little evidence of gravitational fractionation in the lock in zone, the cause of this diffusion has been attributed to dispersion, either driven by closing pores which force out air or by long term changes in pressure at the surface of the snow. Our results indicate that the movement of molecules in the lock in zone is driven by gas diffusivity, and not dispersion.

The measured permeability profile can also provide insight to the understanding of firn air measurements. In the firn air campaign at Summit in 2007, the lock in depth was determined to be 69 m and pore close off was determined to occur at 80 m (Fain et al., 2009). To compare our measurements to these values, we have determined the percentage of impermeable layers at each meter in the deep firn from 60 to 84 m. This

TCD
7, 2455–2487, 2013

was determined by counting the fraction of firn samples within the set of samples in a given meter that yielded a zero permeabiliy in lab experiments. Figure 11 shows a comparison of this parameterization to the lock in zone and pore close off depths determined in the firn air pumping campaign. It appears that the lock in zone begins when approximately 50 % of the firn layers are impermeable. Though there are some samples which have a non-zero permeability below the pore close off point, the difference is reasonable considering the differences in pump characteristics between the laboratory and the field measurements (the lowest measureable permeability in the laboratory is approximately 0.05×10^{-10} m^2), and that the firn air campaigns are sampling air from a larger volume of firn. While a laboratory sample may be impermeable, the larger volume of firn at that depth in the ice sheet may have a limited but existent number of permeable paths that were not represented in the firn core sample. Conversely, having a larger volume of firn air to sample may indicate that the firn is impermeable while there are still some very small permeable layers that can be found in the higher depth resolution laboratory measurements.

4 Conclusions

From a phemonenological investigation of gas transport through firn at Summit, we can draw a number of conclusions, which apply to Summit as a case study. It is a site where the climate has not experienced a lot of change in recent decades, so that the firn has a fairly consistent layering pattern, and there were no melt layers in the firn. We have shown that diffusivity and permeability are not linearly related throughout the entire firn column, though the two are linearly proportional below 40 m. Effect tests have shown that permeability is more sensitive to the firn microstructure than is gas diffusivity. We have shown that measured gas diffusivity of firn is consistently lower than modeled diffusivity from firn air measurements (as was also seen by Fabre et al., 2000). This indicates that there is an additional phenomenon causing apparent gas transport in the firn as revealed by firn air chemistry measurements. The variation between modeled

TCD
7, 2455–2487, 2013

and measured diffusivity is likely caused by a combination of the lateral inhomogeneity in the firn and the time varience of gas transport which is sensitive to the layered nature of firn, since the layers have different physical properties. The diffusivity measurements do not conflict with previous parameterizations of convection in the firn, but they do indicate that molecular diffusion can indeed occur in the lock in zone of firn.

From these conclusions we recommend the following additional research: we encourage firn gas transport modelers to include direct measurements of diffusivity and other physical constraints in the models. As modeled diffusivity is generally higher than our measured values, this will result in a portion of gas trasnport for which there is currently not a physical method of accounting. We suggest research on the effects of lateral inhomogeneity to attempt to fill this gap. Additionally, with measurements of diffusivity and permeability, along with gas concentration profiles, a more physically based representation of the convective zone can be developed with the input of driving surface pressures (as in Albert, 1993, 1996). A similar study at a polar site with different local temperature and average accumulation may illuminate the effects of microstructure on the relationship between diffusivity and permeability and could broaden the applicability of measured parameters in firn air models.

Acknowledgements. We would like to acknowledge Elise Williamson, Noah Pfister, and Zoe Courville for completing a significant portion of the permeability measurements. We would also like to thank Christo Buizert and Mark Battle for sharing their models of gas diffusivity from Summit, Greenland, and thank Jeff Severinghaus and Chriso Buizert for useful conversations. We thank Frank Perron for his construction of laboratory instruments. This research was sponsored by the following grants: NSF-OPP-0520445, NSF-OPP-0944078, and NSF-PIRE-0968391.

References

Adolph, A. and Albert, M. R.: An improved technique to measure firn diffusivity, Int. J. Heat Mass Tran., 61, 598–604, 2013.

Albert, M. R.: Some numerical experiments on firn ventilation with heat transfer, Ann. Glaciol., 18, 161–165, 1993.

TCD

7, 2455–2487, 2013

Albert, M. R.: Modeling heat, mass, and species transport in polar firn, Ann. Glaciol., 23, 138–143, 1996.
Albert, M. R. and Shultz, E. F.: Snow and firn properties and air–snow transport processes at Summit, Greenland, Atmos. Environ., 36, 2789–2797, 2002.
Albert, M. R., Shultz, E. F., and Perron, F. E.: Snow and firn permeability at Siple Dome, Antarctica, Ann. Glaciol., 31, 353–356, 2000.
Blunier, T. and Brook, E. J.: Timing of millennial-scale climate change in Antarctica and Greenland during the last glacial period, Science, 291, 109–112, 2001.
Brook, E. J.: Leads and lags at the end of the last Ice Age, Science, 339, 1042–1043, 2013.
Buizert, C., Martinerie, P., Petrenko, V. V., Severinghaus, J. P., Trudinger, C. M., Witrant, E., Rosen, J. L., Orsi, A. J., Rubino, M., Etheridge, D. M., Steele, L. P., Hogan, C., Laube, J. C., Sturges, W. T., Levchenko, V. A., Smith, A. M., Levin, I., Conway, T. J., Dlugokencky, E. J., Lang, P. M., Kawamura, K., Jenk, T. M., White, J. W. C., Sowers, T., Schwander, J., and Blunier, T.: Gas transport in firn: multiple-tracer characterisation and model intercomparison for NEEM, Northern Greenland, Atmos. Chem. Phys., 12, 4259–4277, doi:10.5194/acp-12-4259-2012, 2012.
Courville, Z. R., Albert, M. R., Fahnestock, M. A., Cathles, L. M., and Shuman, C. A.: Impacts of an accumulation hiatus on the physical properties of firn at a low-accumulation polar site, J. Geophys. Res.-Earth, 112, F02030, doi:10.1029/2005JF000429, 2007.
Courville, Z., Hörhold, M., Hopkins, M., and Albert, M.: Lattice–Boltzmann modeling of the air permeability of polar firn, J. Geophys. Res.-Earth, 115, F04032, doi10.1029/2009JF001549, 2010.
Fabre, A., Barnola, J. M., Arnaud, L., and Chappellaz, J.: Determination of gas diffusivity in polar firn: comparison between experimental measurements and inverse modeling, Geophys. Res. Lett., 27, 557–560, 2000.
Faïn, X., Ferrari, C. P., Dommergue, A., Albert, M. R., Battle, M., Severinghaus, J., Arnaud, L., Barnola, J.-M., Cairns, W., Barbante, C., and Boutron, C. Polar firn air reveals large-scale impact of anthropogenic mercury emissions during the 1970s, P. Natl. Acad. Sci. USA, 106, 16114–16119, 2009.
Freitag, J., Dobrindt, U., and Kipfstuhl, J.: A new method for predicting transport properties of polar firn with respect to gases on the pore-space scale, Ann. Glaciol., 35, 538–544, 2002.
Garboczi, E. J.: Permeability, diffusivity, and microstructural parameters: a critical review, Cement Concrete Res., 20, 591–601, 1990.

TCD
7, 2455–2487, 2013

Garboczi, E. J. and Bentz, D. P.: The effect of statistical fluctuation, finite size error, and digital resolution on the phase percolation and transport properties of the NIST cement hydration model, Cement Concrete Res., 31, 1501–1514, 2001.
Horhold, M. W., Albert, M. R., and Freitag, J.: The impact of accumulation rate on anisotropy and air permeability of polar firn at a high accumulation site, J. Glaciol., 55, 625–630, 2009.
Kawamura, K., Severinghaus, J. P., Ishidoya, S., Sugawara, S., Hashida, G., Motoyama, H., Fujii, Y., Aoki, S., and Nakazawa, T.: Convective mixing of air in firn at four polar sites, Earth Planet. Sc. Lett., 244, 672–682, 2006.
Lomonaco, R., Albert, M., and Baker, I.: Microstructural evolution of fine-grained layers through the firn column at Summit, Greenland, J. Glaciol., 57, 755–762, 2011.
Matsunaga, N., Hori, M., and Nagashima, A.: Diffusion coefficients of global warming gases into air and its component gases, High Temp.-High Press., 30, 77–84, 1998.
Matsunaga, N., Hori, M., and Nagashima, A.: Measurements of the mutual diffusion coefficients of gases by the Taylor method (7th Report, measurements on the SF_6–air, SF_6–N_2, SF_6–O_2, CFC_{12}–N_2, CFC_{12}–O_2, $HCFC_{22}$–N_2 and $HCFC_{22}$–O_2 systems), Trans. Jpn. Soc. Mech. Eng. B, 68, 550–555, 2002.
Nghiem, S. V., Hall, D. K., Mote, T. L., Tedesco, M., Albert, M. R., Keegan, K., Shuman, C. A., DiGirolamo, N. E., and Neumann, G.: The extreme melt across the Greenland ice sheet in 2012, Geophys. Res. Lett., 39, L20502, doi:10.1029/2012GL053611, 2012.
Rick, U. K. and Albert, M. R.: Microstructure and permeability in the near-surface firn near a potential US deep-drilling site in West Antarctica, Ann. Glaciol., 39, 62–66, 2004.
Schwander, J.: The transformation of snow to ice and the occlusion of gases, in: The Environmental Record in Glaciers and Ice Sheets, edited by: Oeschger, H., and Langway Jr., C. C., John Wiley & Sons, New York, 53–67, 1989.
Schwander, J., Stauffer, B., and Sigg, A.: Air mixing in firn and the age of the air at pore close-off, Ann. Glaciol, 10, 141–145, 1988.
Schwander, J., Barnola, J. M., Andrié, C., Leuenberger, M., Ludin, A., Raynaud, D., and Stauffer, B.: The age of the air in the firn and the ice at Summit, Greenland, J. Geophys. Res., 98, 2831–2838, 1993.
Severinghaus, J. P., Grachev, A., and Battle, M.: Thermal fractionation of air in polar firn by seasonal temperature gradients, Geochem. Geophy. Geosy., 2, 2000GC000146, doi:10.1029/2000GC000146, 2001.

TCD
7, 2455–2487, 2013

Severinghaus, J. P. and Battle, M. O.: Fractionation of gases in polar ice during bubble close-off: new constraints from firn air Ne, Kr and Xe observations, Earth Planet. Sc. Lett., 244, 474–500, 2006.

Severinghaus, J. P., Beaudette, R., Headly, M. A., Taylor, K., and Brook, E. J.: Oxygen-18 of O_2 records the impact of abrupt climate change on the terrestrial biosphere, Science, 324, 1431–1434, 2009.

Sowers, T., Bender, M., Raynaud, D., and Korotevich, Y. S.: $\Delta^{15}N$ of N_2 in air trapped in polar ice: a tracer of gas transport in the firn and a possible constraint on ice age-gas age differences, J. Geophys. Res.-Atmos., 97, 15683–15697, 1992.

Trudinger, C. M., Enting, I. G., Rayner, P. J., Etheridge, D. M., Buizert, C., Rubino, M., Krummel, P. B., and Blunier, T.: How well do different tracers constrain the firn diffusivity profile?, Atmos. Chem. Phys., 13, 1485–1510, doi:10.5194/acp-13-1485-2013, 2013.

Witrant, E., Martinerie, P., Hogan, C., Laube, J. C., Kawamura, K., Capron, E., Montzka, S. A., Dlugokencky, E. J., Etheridge, D., Blunier, T., and Sturges, W. T.: A new multi-gas constrained model of trace gas non-homogeneous transport in firn: evaluation and behaviour at eleven polar sites, Atmos. Chem. Phys., 12, 11465–11483, doi:10.5194/acp-12-11465-2012, 2012.

TCD
7, 2455–2487, 2013

Table 1. Results of effect tests on linear standard least squares fit models showing the relative effect of each input parameter and the p value for each effect test in parenthesis.

	Porosity	SSA	Average Pore Diameter
Normalized Diffusivity	86.7 % (0.0006)	7.7 % (0.25)	5.5 % (0.33)
$\log_{10}$ Permeability	59.7 % (< 0.0001)	31.3 % (0.003)	9.0 % (0.0901)

TCD
7, 2455–2487, 2013

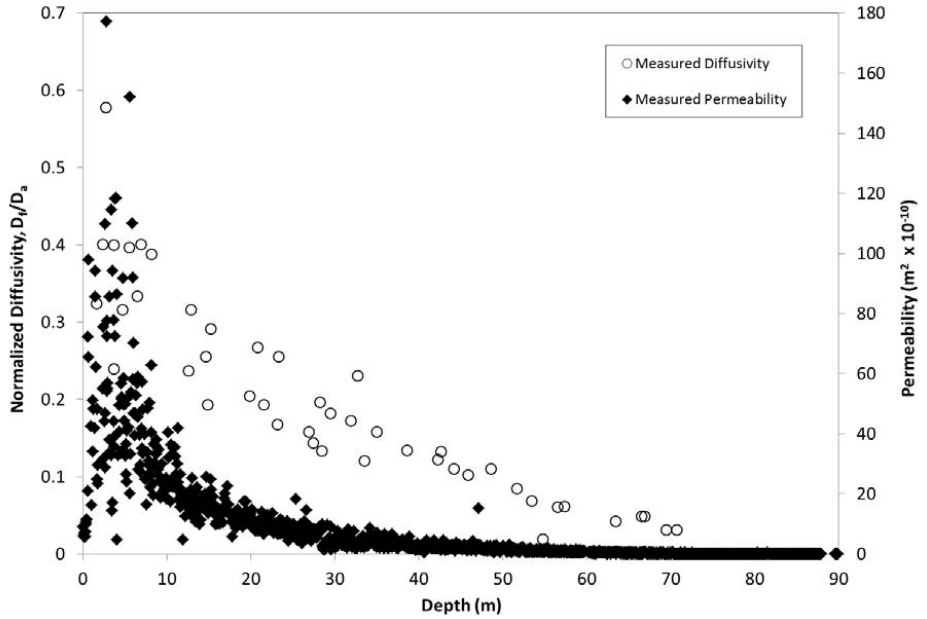

Fig. 1. Normalized diffusivity and permeability vs. depth for discrete firn samples from Summit, Greenland.

TCD
7, 2455–2487, 2013

The physical basis for gas transport through polar firn

A. C. Adolph and M. R. Albert

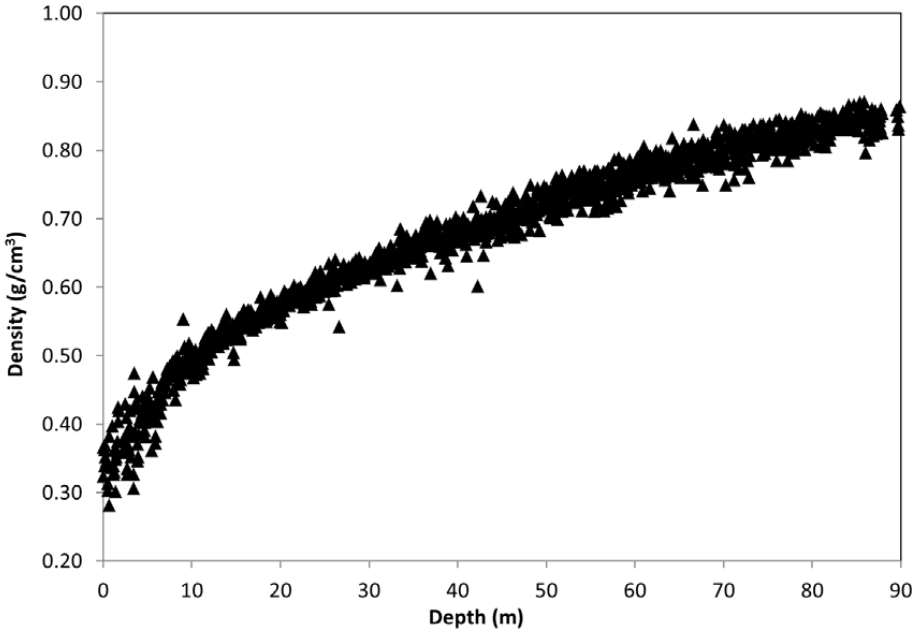

Fig. 2. Density profile for the firn at Summit, Greenland.

TCD
7, 2455–2487, 2013

The physical basis for gas transport through polar firn

A. C. Adolph and M. R. Albert

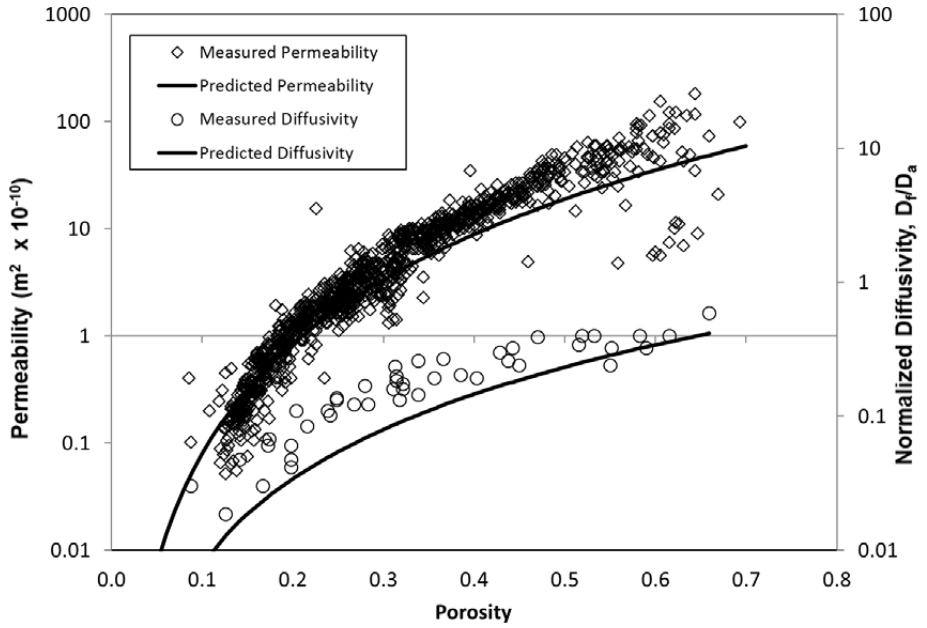

Fig. 3. Permeability and normalized diffusivity plotted against porosity, showing the predicted permeability and diffusivity formulas developed by Freitag et al. (2002) using lattice Boltzmann modeling.

TCD
7, 2455–2487, 2013

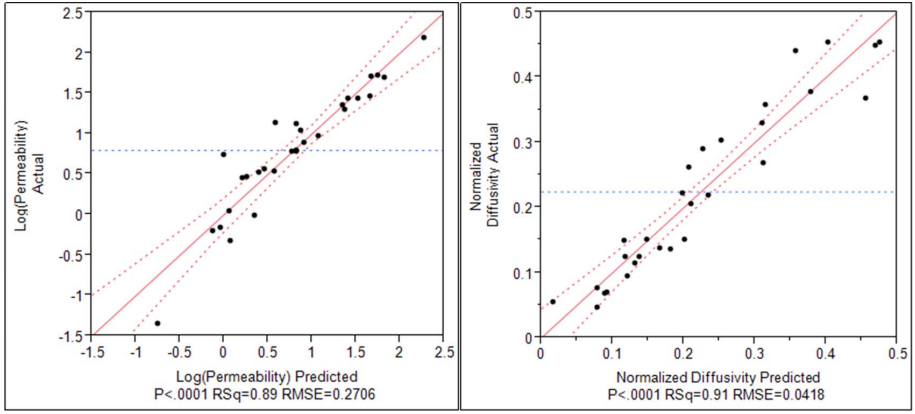

Fig. 4. Results of linear standard least squares fit model for the logarithm of permeability and the normalized diffusivity, where porosity, specific surface area and average pore diameter are used as model inputs.

TCD
7, 2455–2487, 2013

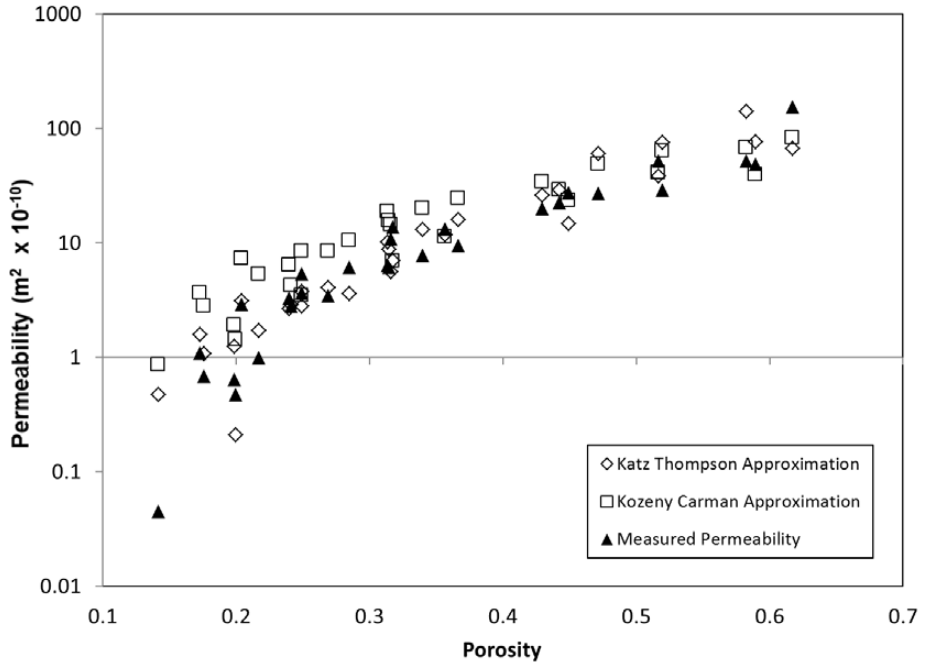

Fig. 5. Measured permeability compared to Kozeny–Carman and Katz–Thompson approximations.

TCD
7, 2455–2487, 2013

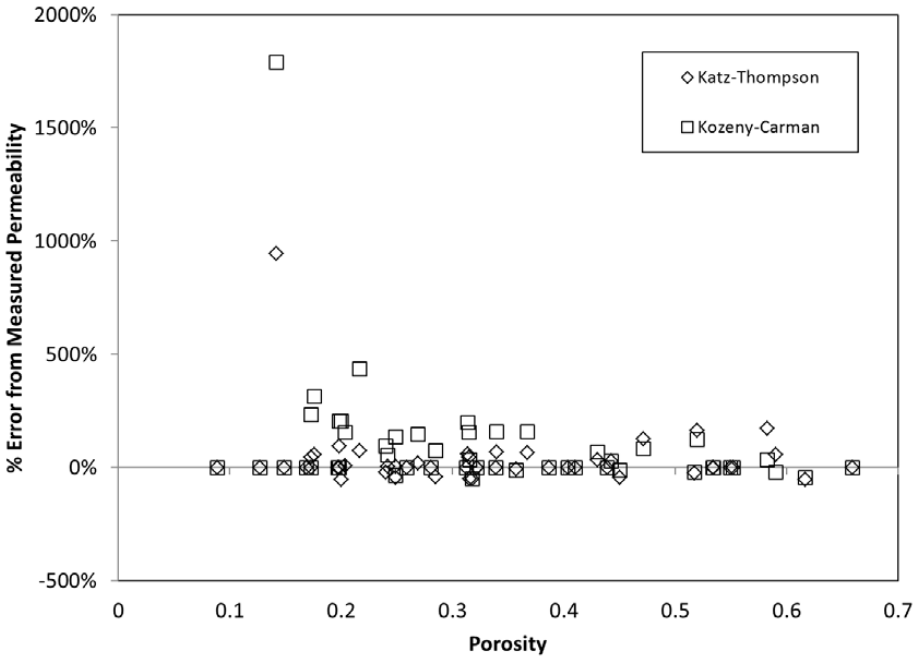

Fig. 6. Percent error between approximated permeability and measured permeability across the range of porosities considered.

TCD
7, 2455–2487, 2013

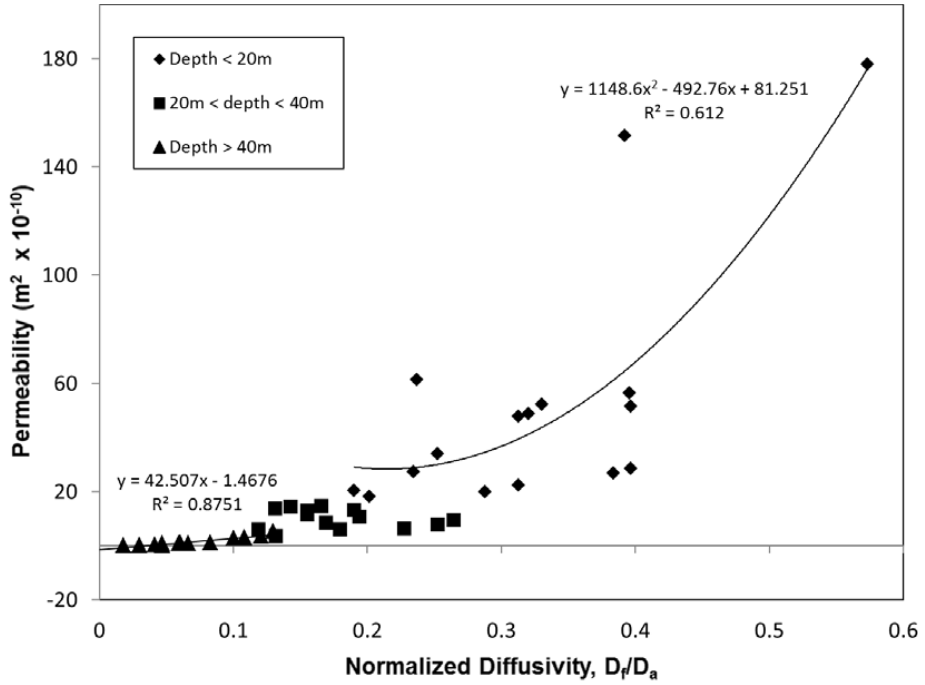

Fig. 7. Permeability vs. normalized diffusivity showing the demarcations between positive SMI (depth < 20 m), variably positive and negative SMI (depth between 20 m and 40 m) and negative SMI (depth > 40 m). The nature of the relationship between diffusuvity and permeability appears to change with these shifts in concavity or convexity of the structure.

TCD
7, 2455–2487, 2013

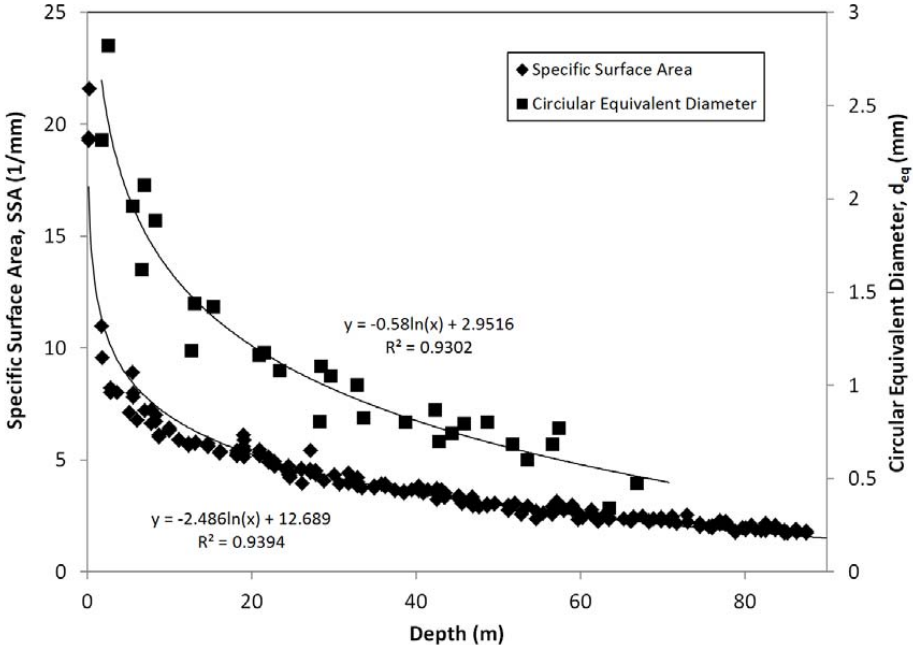

Fig. 8. Average equivalent circle diameter of pores and SSA vs. depth. The d_{eq} and SSA drop quickly in the near surface, and then the rate of change lowers significantly with depth, following a logarithmic function.

TCD
7, 2455–2487, 2013

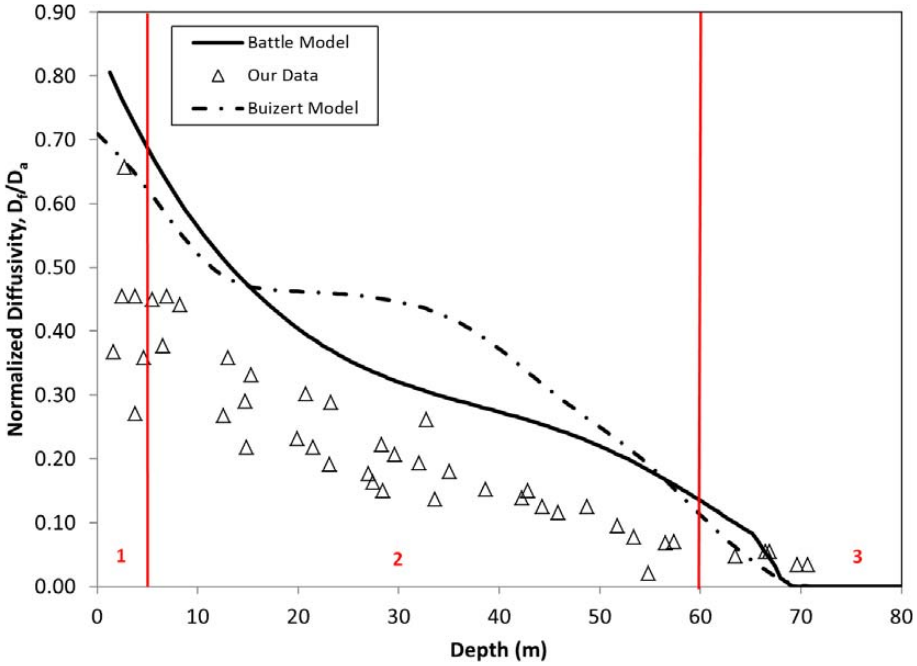

Fig. 9. Comparison of measured diffusivity to diffusivity modeled from firn air measurements. Lines show separations of regions, considering the differnt causes for deviation between measured and modeled results.

TCD
7, 2455–2487, 2013

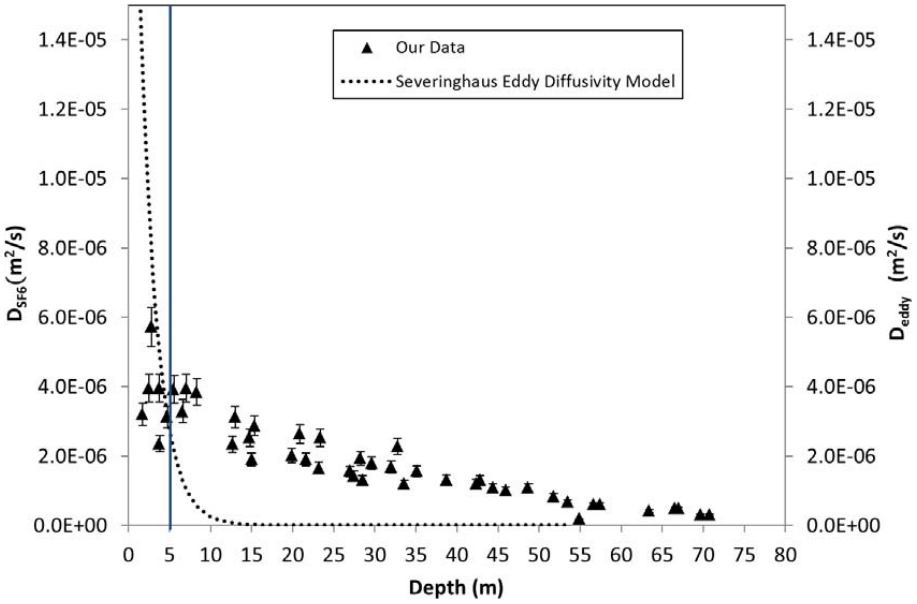

Fig. 10. Diffusivity of SF_6 as determined in lab experiments compared to the eddy diffusion parameterization of near surface firn at Summit (J. Severinghaus, personal communication, 2012)

TCD
7, 2455–2487, 2013

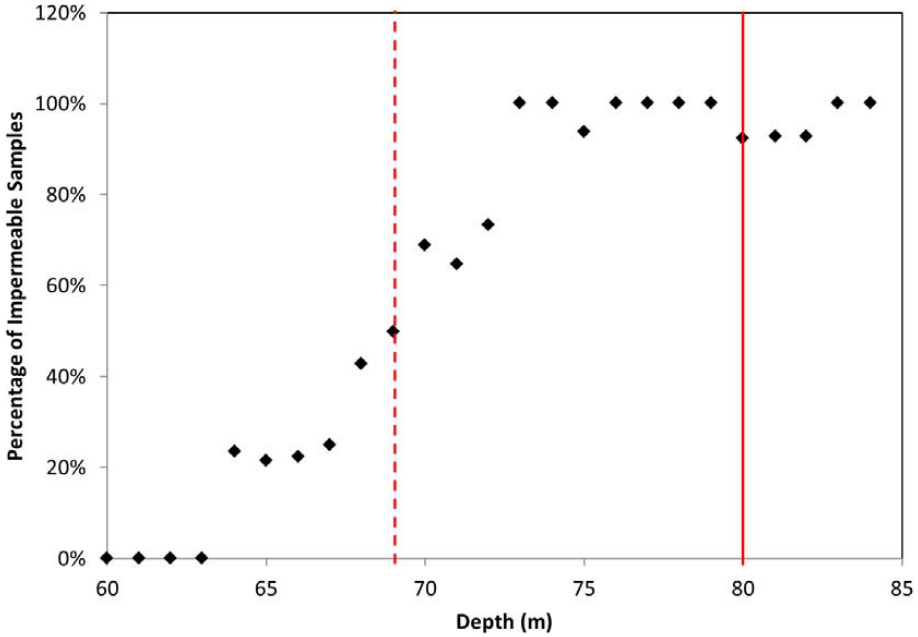

Fig. 11. Percentage of impermeable samples within the set for a given meter. The figure shows the start of the lock in zone (dashed line) and the point of pore close off (solid line) as determined by firn air measurements (Fain et al., 2009).

TCD
7, 2455–2487, 2013